Two-state intermittency near a symmetric interaction of saddle-node and Hopf bifurcations: a case study from dynamo theory

Peter Ashwin[*]

Department of Mathematical Sciences, Laver Building,
University of Exeter, Exeter EX4 4QE, UK

Alastair M. Rucklidge[†]and Rob Sturman[‡]
Department of Applied Mathematics, University of Leeds,
Leeds LS2 9JT, UK

September 25, 2003

Abstract

We consider a model of a Hopf bifurcation interacting as a codimension 2 bifurcation with a saddle-node on a limit cycle, motivated by a low-order model for magnetic activity in a stellar dynamo. This model consists of coupled interactions between a saddle-node and two Hopf bifurcations, where the saddle-node bifurcation is assumed to have global reinjection of trajectories. The model can produce chaotic behaviour within each of a pair of invariant subspaces, and also it can show attractors that are *stuck-on* to both of the invariant subspaces. We investigate the detailed intermittent dynamics for such an attractor, investigating the effect of breaking the symmetry between the two Hopf bifurcations, and observing that it can appear via blowout bifurcations from the invariant subspaces.

We give a simple Markov chain model for the two-state intermittent dynamics that reproduces the time spent close to the invariant subspaces and the switching between the different possible invariant subspaces; this clarifies the observation that the proportion of time spent near the different subspaces depends on the average residence time and also on the probabilities of switching between the possible subspaces.

[*]P.Ashwin@ex.ac.uk

[†]A.M.Rucklidge@leeds.ac.uk

[‡]rsturman@maths.leeds.ac.uk

1 Introduction

Modelling chaotic and intermittent changes, for example in the intensity and polarity of magnetic fields caused by stellar dynamos, is a significant challenge, whether via minimal phenomenological models, mean-field models or detailed numerical simulations. Previous work of Tobias *et al.* [28] and Knobloch *et al.* [16] in this direction used the dynamics near an interaction of local bifurcations (saddle-node and Hopf) to suggest low-order phenomenological models for the stellar dynamo problem. The interaction of saddle-node and Hopf bifurcations is one of the simplest bifurcations that gives rise to chaotic attractors local to the bifurcation [12] and hence is useful in providing a model with chaotic behaviour in a truncated bifurcation normal form.

One aim of the present paper is to combine and modify aspects of the models to overcome one of the main problems in [16, 28], namely the fact that the attractors there are only marginally stable and small changes to initial conditions or parameters lead to solutions that depart to infinity. We do this by assuming that the saddle-node bifurcation occurs on a limit cycle [1, 14], and so ensure that the dynamics will remain in a compact region in phase space; this allows much more robust simulation of the dynamics than was possible in [16, 28]. We remark that the saddle-node/Hopf bifurcation with global reinjection has been subject of recent study by [17, 18] and shows very rich bifurcation and periodic orbit structure. We will be mostly concerned with the case in which there is a chaotic attractor for two such bifurcations, symmetrically coupled.

The model (4) we derive in Section 2 consists of ordinary differential equations (ODEs) in six (real) variables. Symmetries force the existence of two invariant subspaces of three dimensions; these correspond to pure dipole and pure quadrupole magnetic fields in the analogous model of [16]. The intersection of the two subspaces is of one dimension and this is the variable that undergoes the saddle-node bifurcation. The dynamics within each of the three-dimensional subspaces can be chaotic, and attractors may include points within (or be 'stuck on' to) these subspaces and hence typical trajectories show intermittency where they remain for arbitrarily long times in arbitrarily small neighbourhoods of the invariant subspace. This leads to the appearance of on–off and other types of intermittency; see for example [11, 13, 19, 20, 26]; for reviews, see for example [5, 24].

This leads on to the second aim of the paper; to investigate in detail some examples of intermittent dynamics of some attractors for the model (4) where the dynamics is intermittent to more than one invariant subspace. Although intermittent dynamics has been found previously in examples of mean field dynamos, as far as we are aware this is the first example of two-state intermittency in such a model that involves chaotic saddles within the invariant subspaces. To this end, we look at numerical simulations typical for the system in Section 3 and consider their intermittent dynamics in detail.

Previous examples of *two-state intermittency* include, for example, [3] and [10, 29], where attractors are on–off intermittent to more than one invariant subspace such that the same chaotic saddle governs approach towards and departure from the invariant subspace. Here we find *in–out*

intermittency (see [5]) where different saddles are responsible for approach towards and departure from the subspace. This in–out intermittency has previously been found in PDE and ODE dynamo models [9] and in other situations [19] but not as a *two-state* intermittency.

In particular, the dynamics of the intermittent attractor explores a neighbourhood of the invariant subspace that includes the attractor within the invariant subspace, but which also includes unstable dynamics within the subspace. We briefly investigate the appearance of two-state intermittency via blowout bifurcations from the invariant subspaces (cf. for example [2, 3, 11, 22, 23]) and find evidence that subcritical blowout bifurcations from the invariant subspaces is succeeded by a crisis that sets up two-state in–out intermittency.

Section 4 models two-state intermittency in the model (4) via the probability density of a Markov model for the distance from each of the invariant subspaces. We use this to obtain estimates for the proportion of time spent near each of the invariant subspaces, and fit the parameters in the model to the numerical examples in previous sections. Finally in Section 5 we discuss some generalities of the model and its dynamics, and of the probabilistic model.

2 Formulation of the model

The main model we study in this paper is a system of six coupled ODEs with two invariant subspaces each of three dimensions; these represent pure dipole and pure quadrupole magnetic fields in the motivating models [16, 28] for this work. The intersection of these invariant subspaces is a one dimensional ODE corresponding to zero magnetic field.

We aim in this paper to improve the models of [16] and [28] to (a) allow chaotic behaviour within the symmetric subspaces, (b) make the appearance of two-state intermittent attractors between these subspaces more robust and (c) avoid problems with sensitivity to parameters and initial condition that may lead to blowing up in [16], by making the 'zero magnetic field' variable compact. We defer a detailed discussion of the motivation of the model, and the differences from the models of [16] and [28] to section 2.6.

2.1 Saddle-node/Hopf bifurcation

We consider a codimension 2 bifurcation. The interaction of a saddle-node bifurcation and a Hopf bifurcation is well understood [12]. This occurs when the Jacobian matrix of a flow has a pure imaginary pair and a simple zero eigenvalue. This can be written in normal form, truncated to quadratic order, as

$$\begin{aligned} \dot{z} &= (\mu + i\omega)z + \epsilon z v \\ \dot{v} &= \kappa - v^2 + e_1|z|^2 \end{aligned} \tag{1}$$

where $z \in \mathbb{C}$, $v \in \mathbb{R}$, and $\mu, \omega, \epsilon, \kappa, e_1 \in \mathbb{R}$ are parameters. A normal form symmetry is present in the equations, namely $z \to z e^{i\phi}$, for any fixed angle ϕ. (This includes the symmetry $z \to -z$.)
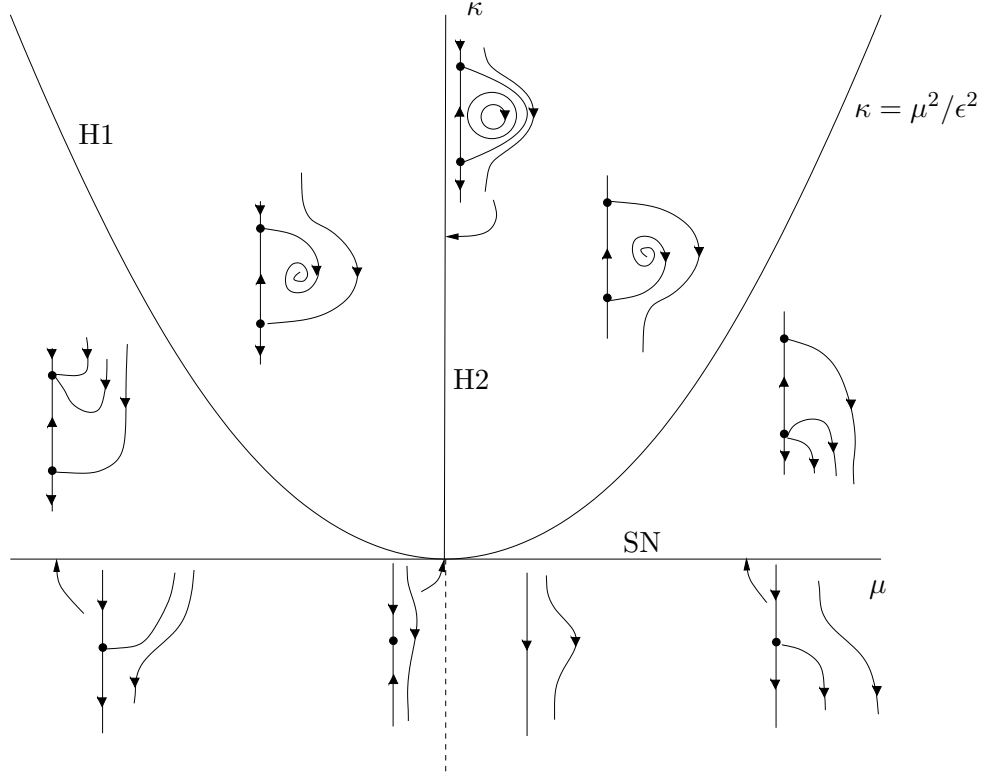
Figure 1: Bifurcation diagram for the degenerate case (1) of the interaction of a saddle-node bifurcation (marked SN, unfolding parameter κ) and a Hopf bifurcation (marked H1, unfolding parameter μ). Observe that there is also a heteroclinic connection on the line marked H2, and this is degenerate in that an open set in the phase space is foliated with tori for these parameter values. See the text and [12] for more details.

The parameter e_1 is frequently rescaled to $e_1 = -1$ (the negative sign ensures the Hopf bifurcation is supercritical) [12] and we will take $e_1 = -1$ throughout. A saddle-node bifurcation occurs in the v-direction as κ passes through 0, giving fixed points, v_+ and v_-, at $(z, v) = (0, \pm\sqrt{\kappa})$. The system is axisymmetric because of the normal form symmetry, and so can be transformed into cylindrical polars $(r, \theta, v) = (|z|, \arg(z), v)$ with the angular variable decoupled. A limit cycle $\mathcal{L}$ at $(r, v) = (\sqrt{\kappa - \mu^2/\epsilon^2}, -\mu/\epsilon)$ for $\mu^2 \leq \epsilon^2 \kappa$ is created as the complex variable z undergoes a Hopf bifurcation on crossing the line $\kappa = \mu^2/\epsilon^2$. A heteroclinic connection $\mathcal{H}$ from v_+ to v_- exists at $\kappa = 0$ ($\mu > 0$). This indicates a degenericity in the model, since also on this half-line there is a secondary Hopf bifurcation, in which the limit cycle bifurcates into a nested family of tori. The behaviour of the system is summarized in figure 1, for the case $\epsilon > 0$ (see [12] for details).

This system models a dynamo in which hydrodynamic behaviour (with magnetic field equal to zero) is represented by the v-axis. The properties of a dynamo require that this axis remain invariant. Two different convecting states (one hydrodynamically stable but magnetically unstable,

4

and one hydrodynamically unstable but magnetically stable) are represented by the two fixed points on the v-axis. The complex coordinate z represents the magnetic field. When separated into real and imaginary parts we have a natural correspondence of real part with the toroidal field, and imaginary part with the poloidal field [28]. The (primary) supercritical Hopf bifurcation represents the onset of magnetic instability. Also in the $\dot{z}$ equation is a term giving the contribution of the velocity field to the magnetic flux. (This is the only permissible quadratic term, since v^2 would break the invariance of the v-axis, and $|z|^2$ would break the invariance $z \rightarrow -z$, needed to allow a reversal of the field.) Finally, the v equation also contains a term modelling the Lorentz force (reaction of the magnetic field) on the flow.

There is an open set of initial conditions for which trajectories escape to $v = -\infty$. In particular, trajectories that begin outside the heteroclinic connection $\mathcal{H}$ escape in this way. This can be prevented by introducing another attracting fixed point on the v-axis, near $-\infty$ [28]. This also results in the degeneracy of the secondary Hopf being broken.

2.2 Breaking the degeneracy of the secondary Hopf

Adding a cubic term cv^3 to the $\dot{v}$ equation retains the axisymmetry, breaks the secondary Hopf degeneracy, and introduces a new fixed point at $v \approx 1/c$. Thus the system becomes

$$
\begin{aligned}
\dot{z} &= (\mu + i\omega)z + \epsilon zv \\
\dot{v} &= \kappa - v^2 + cv^3 - |z|^2.
\end{aligned}
$$

The constant c is chosen to be negative to make the new fixed point v_{--} stable in the v-direction. The two original fixed points remain near v_+ and v_- for small c. The bifurcation diagram remains similar to the case above, but now the secondary Hopf bifurcation no longer occurs at the same parameter values as the existence of $\mathcal{H}$. We also have regions of parameter space created in which stable two-tori are possible (see [12, 15] for details).

2.3 Breaking the axisymmetry

The axisymmetry of the system, which is a normal form symmetry, allows the angular component to be decoupled, and so the system is two-dimensional in the remaining variables. Thus no chaotic dynamics is possible. Breaking the axisymmetry allows more complicated trajectories to occur. The system as a dynamo model also demands that the axisymmetry is broken, as it implies the equivalence of the poloidal and toroidal fields, which is not true for the dynamo process. However, changing the sign of the magnetic field is a symmetry of the dynamo problem. We break this symmetry in a way that preserves the invariance of the v-axis and retains the symmetry $z \rightarrow -z$, by adding a term proportional to z^3. (The symmetry $z \rightarrow -z$ is erroneously absent from the model

in [28].)

$$\begin{aligned}
\dot{z} &= (\mu + i\omega)z + \epsilon z v + dz^3 \\
\dot{v} &= \kappa - v^2 + cv^3 - |z|^2
\end{aligned} \qquad (2)$$

Although this results in a system with a degree of non-genericity (the invariance of the v-axis), this constraint is required for the system to be a viable model of a dynamo — any purely hydrodynamic states must remain purely hydrodynamic for all time.

2.4 Preventing escape of trajectories to infinity

In order to prevent solutions from escaping to $v = -\infty$ *or* being attracted to a fixed point near $-\infty$, we can render the system periodic in v. On the v-axis, instead of a saddle-node bifurcation on an infinite line, we have a saddle-node bifurcation on a limit cycle. Any trajectories threatening to escape close to the lower unstable manifold of v_- return close to the upper stable manifold of v_+: we call this process the global reinjection. This type of reinjection of solutions has been studied in many models, and its interaction with a Hopf bifurcation is studied in [17, 18], for models of optically driven lasers.

We choose to make v periodic on the interval $[\pi L/2, \pi L/2]$, where L is a new parameter. In order to ensure that the v variable and its powers remain continuous on this interval, we observe that we need trigonometric functions that are (a) periodic on $[-\pi L/2, \pi L/2]$, and (b) proportional to v, v^2, and v^3 for v close to 0. Set $u_1 = L \sin(v/L)$, so that for sufficiently small v, $u_1 \approx v$. Similarly, set $u_2 = \frac{L}{2} \sin \frac{2v}{L}$: for small v, $u_2 \approx v$ as well. The new variable u_1 is not periodic on $[\pi L/2, \pi L/2]$, but u_2 and u_1^2 are, as is $u_1^2 u_2$. The system can thus be made periodic and continuous by substituting

$$\begin{aligned}
v &\rightarrow u_2 \\
v^2 &\rightarrow u_1^2 \\
v^3 &\rightarrow u_1^2 u_2
\end{aligned}$$

and confining v to the interval $[-\pi L/2, \pi L/2]$. Hence the full system becomes

$$\begin{aligned}
\dot{z} &= (\mu + i\omega)z + \epsilon z u_2 + dz^3 \\
\dot{v} &= \kappa - u_1^2 + cu_1^2 u_2 - |z|^2
\end{aligned} \qquad (3)$$

with $u_1 = L \sin(v/L)$ and $u_2 = \frac{L}{2} \sin \frac{2v}{L}$.

This system can produce, for suitable parameter choices, all the behaviour discussed in [28], with the added advantage that nearly all trajectories remain in a compact region of phase space. In particular, the secondary Hopf bifurcation creates quasiperiodic behaviour in the form of an attracting two-torus. Increasing the linear growth term μ triggers a breaking down of the two-torus and a transition to chaos. During this transition, parameter values exist at which typical trajectories are attracted to frequency-locked limit cycle. In fact, parameter values exist at which
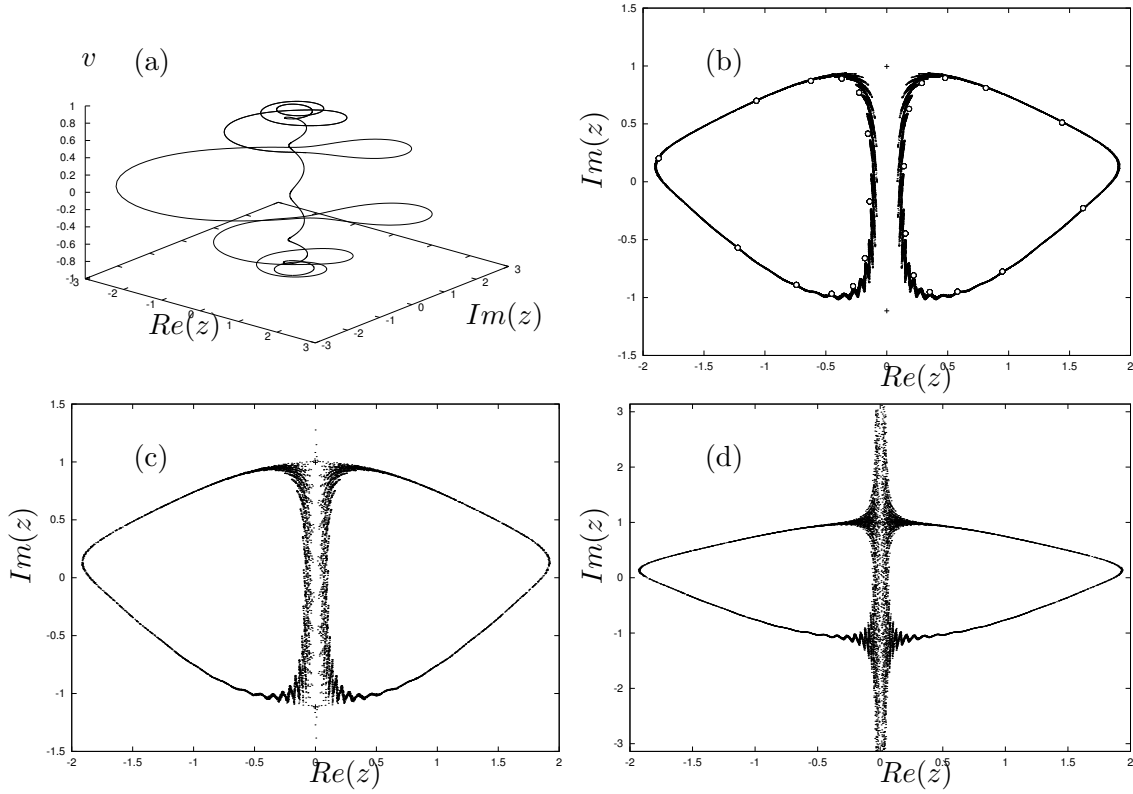
Figure 2: Attractors for the system (3) on increasing μ, with other parameters $\omega = 10.0$, $\epsilon = 1.0$, $d = 4.9$, $\kappa = 1.0$, $c = -0.1$, $L = 2.0$. In (a) $\mu = 0.026$ we have a stable periodic orbit, with the trajectory winding twelve times around the v-axis during one full period. In (b) $\mu = 0.026$ again, but different initial conditions give a chaotic attractor. This is a Poincaré section through $Im(z) = 0$. Superimposed are circles representing the periodic solution of (a). The equilibria (indicated by crosses) are located at $(Re(z), v) = (0, 0.966)$, $(0, -1.114)$. In (c) $\mu = 0.027$, and the chaotic attractor gets closer to the v-axis. Finally in (d), with $\mu = 0.028$, reinjections are common and the trajectory spends a long time with $|z|$ very small.

chaotic motion is bistable with periodic attractors. Figure 2(a) shows a periodic attractor for parameter values $\mu = 0.026$, $\omega = 10.0$, $\epsilon = 1.0$, $d = 4.9$, $\kappa = 1.0$, $c = -0.1$, $L = 2.0$. The trajectory winds twelve times around the v-axis during one full period. Similar limit cycles appear at smaller values of μ, apparently for most initial conditions. At these parameter values however, the basin of attraction for this limit cycle seems very small. Most initial conditions lead to chaotic motion illustrated in figure 2(b). This is a Poincaré section formed by plotting $(Re(z), v)$ when the trajectory hits the section $Im(z) = 0$. The parameter values are as above, but for different initial conditions. It shows the heteroclinic tangle caused by the unstable manifold of v_+ crossing the stable manifold of v_-. (The fixed points v_+ and v_- are given by crosses on figures 2(b), (c) and (d).) Superimposed on the chaotic solution are circles plotted where the periodic orbit of figure 2(a) crosses the Poincaré section. Increasing μ further allows the chaotic attractor to much smaller values of $|z|$, close to the v-axis, owing to the heteroclinic connection and the reinjection mechanism. Figure 2(c) shows an attractor for $\mu = 0.027$. Here very occasional reinjections are required. When the trajectory reaches $v = -\pi L/2 = -\pi$ it is reinjected at $v = \pi$. Figure 2(d) shows an attractor for $\mu = 0.028$. At this parameter the trajectory makes a reinjection roughly as often as it travels up the v-axis. This is as close as the attractor will get to $|z| = 0$, as increasing μ further results in a move away from the v-axis, as reinjections become more common and eventually inevitable.

2.5   Interaction of saddle-node bifurcation with two Hopf bifurcations

We now introduce a second transverse complex direction and assume there are Hopf bifurcations in each of the variables z_1 and z_2. We include an equation representing an antisymmetric velocity component, w along the lines of [16] giving the 6-dimensional system that we consider for the rest of this paper.

$$
\begin{aligned}
\dot{z}_1 &= (\mu + \sigma + i\omega_1)z_1 + \epsilon_1 z_1 u_2 + d_1 z_1^3 + b_1|z_2|^2 z_1 + (\beta_1 + \gamma_1 u_1^2)w z_2 \\
\dot{z}_2 &= (\mu + i\omega_2)z_2 + \epsilon_2 z_2 u_2 + d_2 z_2^3 + b_2|z_1|^2 z_2 + (\beta_2 + \gamma_2 u_1^2)w z_1 \\
\dot{v} &= \kappa - u_1^2 + cu_1^2 u_2 - (|z_1|^2 + |z_2|^2) \\
\dot{w} &= -\tau w + e(z_1\bar{z}_2 + z_2\bar{z}_1),
\end{aligned} \tag{4}
$$

where μ, σ, $\omega_{1,2}$, $\epsilon_{1,2}$, $d_{1,2}$, $b_{1,2}$, $\gamma_{1,2}$, κ, c, τ, $e \in \mathbb{R}$ and $\beta_{1,2} \in \mathbb{C}$ are all parameters. This system of ODEs has symmetries

$$
\begin{aligned}
\mathcal{S}_1 &: \quad (z_1, z_2, v, w) \to (-z_1, z_2, v, -w) \\
\mathcal{S}_1\mathcal{S}_2 &: \quad (z_1, z_2, v, w) \to (z_1, -z_2, v, -w) \\
\mathcal{S}_2 &: \quad (z_1, z_2, v, w) \to (-z_1, -z_2, v, w)
\end{aligned}
$$

and in the case that $\sigma = 0$ and the parameters are independent of their subscripts, there is an additional symmetry $z_1 \leftrightarrow z_2$. In the general case there are three dimensional invariant subspaces

given by

$$\mathcal{D} = \{(z_1, 0, v, 0)\} \text{ and } \mathcal{Q} = \{(0, z_2, v, 0)\}, \tag{5}$$

and the intersection of these $\mathcal{D} \cap \mathcal{Q}$ corresponding to $z_1 = z_2 = w = 0$.

We have not attempted to include all possible parameters that will unfold the system to any particular order; merely we have included parameters such that the observed dynamics appears to be robust. Note that the presence of the symmetries imply that the global reinjection occurs within the invariant subspace $\mathcal{D} \cap \mathcal{Q}$ and so is persistent as a global connection.

2.6 Interpretation and motivation

The physical motivation behind this model comes from stellar dynamo theory. Mean-field models of stellar dynamos often exhibit oscillatory instabilities to magnetic fields with dipole or quadrupole symmetry: fields that either change sign or that are left invariant by reflections in the equatorial plane of the star. In these models, the instabilities to dipole and quadrupole dynamos occur for similar parameter values and produce similar nonlinear behaviour (apart from symmetry type). The complex variables z_1 and z_2 represent dipole and quadrupole magnetic fields, with the real and imaginary parts representing toroidal and poloidal components of the field, and the near-equivalence of dipole and quadrupole modes is represented by having $|\sigma| \ll \mu$, $\omega_1 \approx \omega_2$, $d_1 \approx d_2$, $b_1 \approx b_2$, $\beta_1 \approx \beta_2$ and $\gamma_1 \approx \gamma_2$. The interaction of non-chaotic dipole and quadrupole dynamos was considered in [16] using a model similar to (4), but with $d_1 = d_2 = 0$.

Real stellar dynamos (and most obviously the Solar dynamo) show behaviour that is not simply oscillatory, but consists of oscillations that are modulated chaotically over a time-scale many times longer than the basic period of the oscillation. The chaotic modulation of a dipole dynamo was considered in [28] using a model similar to (2).

Effectively, we have extended the dipole-quadrupole model of [16] to include the chaotic modulation of [28], by including cubic terms to break axisymmetry. We have also made the model more robust by making v periodic, preventing trajectories from escaping to infinity.

3 Intermittent attractors for the model

We now turn to an investigation of the properties of the model (4). In particular, we are interested in how the chaotic modulation of [28] influences the intermittent switching between dipole and quadrupole activity observed by [16]. In this section we show some numerical results and their interpretation in terms of forms of intermittency. Dynamics is possible which spends time close to each of the invariant subspaces $\mathcal{D}$ and $\mathcal{Q}$ in turn. Throughout this paper we fix some parameters as follows except where explicitly stated:

$$\begin{aligned} &\omega_1 = \omega_2 = 10.0, \ \epsilon_1 = \epsilon_2 = 1, \ \kappa = 1, \ c = -0.1, \ e = 1.0, \\ &\tau = 1.0, \ L = 2, \ \mu = 0.026, \ \sigma = 0.0 \ \text{ and } \ d_1 = d_2 = 4.9. \end{aligned} \tag{6}$$
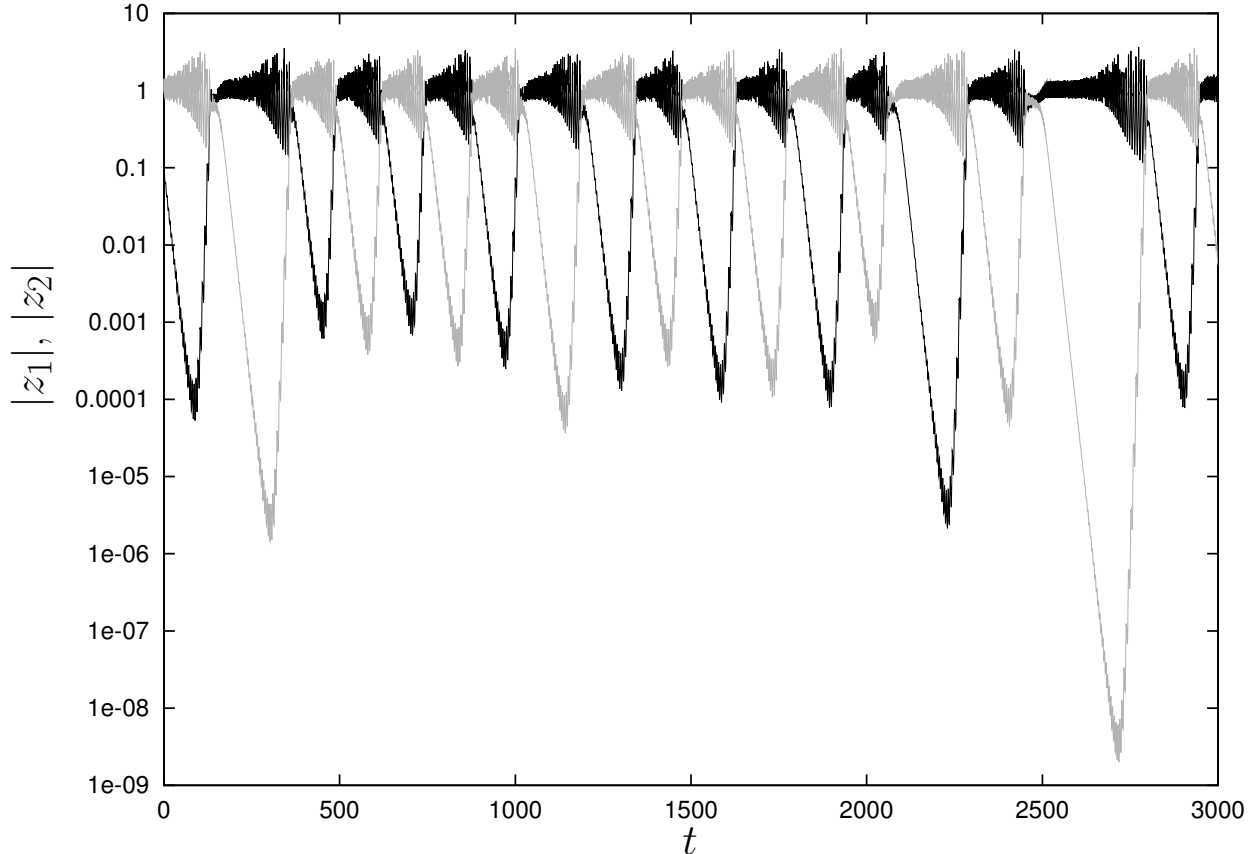
Figure 3: Time series for symmetric parameters showing switching between invariant subspaces: $\mu = 0.026, \sigma = 0$. The black line denotes $|z_1|$ and grey $|z_2|$. The time intervals between intermittent visits close to $\mathcal{D}$ and $\mathcal{Q}$ are apparently random, with a preference for alternating, but have a well-defined mean. The symmetry in the parameters mean that on average an equal time is spent near each invariant subspace.

Recall that L governs the distance between v_+ and v_- via the reinjection, and hence $L = 2$ means that the distance between the fixed points in either direction is comparable. We set the nonlinear coupling parameters as

$$\beta_1 = \beta_2 = -0.5 + 0.5\mathbf{i}, \ \ \gamma_1 = \gamma_2 = 2.5, \ \ b_1 = b_2 = -0.1. \tag{7}$$

3.1 A numerical example of two-state in–out intermittency

With these symmetric parameters ($\sigma = 0$) we can find trajectories which alternate between visiting regions very close to $\mathcal{D}$ and $\mathcal{Q}$, as shown in figure 3. The dynamics is interpreted as follows, using figure 4 as a schematic guide. As the trajectory nears $\mathcal{D}$ (resp. $\mathcal{Q}$), the active variable z_1 (resp. z_2) approaches some invariant (periodic) dynamics D^{in} (resp. Q^{in}) within that subspace, whilst the
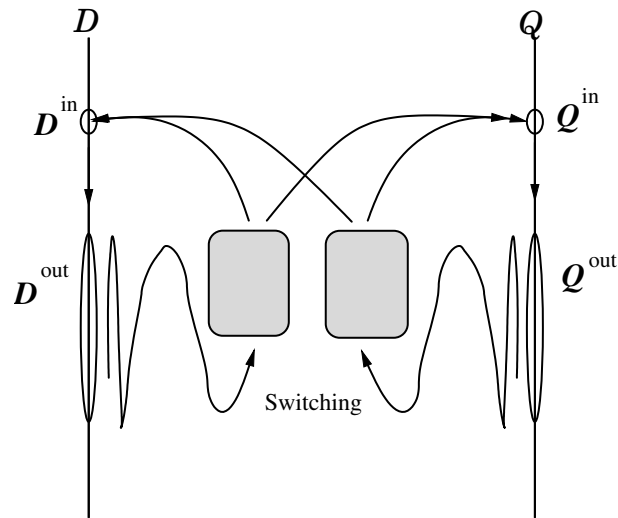
Figure 4: A schematic diagram showing the two-state in–out intermittency observed in Figure 3. The dynamics switches between laminar phases where it remains close to each of the subspaces $\mathcal{Q}$ and $\mathcal{D}$. The approach to the subspace, say $\mathcal{Q}$, is close to the stable manifold of a periodic orbit $\mathcal{Q}^{\text{in}}$ that is unstable within $\mathcal{Q}$ to a chaotic attractor $\mathcal{Q}^{\text{out}}$ with a positive transverse Lyapunov exponent; trajectories then move away from $\mathcal{Q}$ while remaining close the the unstable set of $\mathcal{Q}^{\text{out}}$. When reaching a state of approximately the same distance from $\mathcal{Q}$ and $\mathcal{D}$, the nonlinear dynamics can send the trajectory either back towards $\mathcal{Q}$ or $\mathcal{D}$ in a seemingly random manner.

quiescent variable z_2 (resp. z_1) is suppressed. The dynamics in D^{in} (resp. Q^{in}) within $\mathcal{D}$ (resp. $\mathcal{Q}$) is unstable to another (chaotic) invariant set D^{out} (resp. Q^{out}). When the system is in this state, the quiescent variable is allowed to grow. When the quiescent variable has grown to a similar magnitude to the active variable, a nonlinear switching mechanism sends the system back towards either $\mathcal{D}$ or $\mathcal{Q}$ in a seemingly random manner but with a preference for a switch between $\mathcal{D}$ and $\mathcal{Q}$. The time intervals between switches appear random, but have a well-defined mean. Indeed, for these symmetric parameters, on average an equal amount of time is spent near each invariant subspace. Note that here the dynamics appear to flip almost every time quiescent variables grows to a comparable magnitude as the active variable, but there are occasions when the variables fail to switch and an active dipole (say) phase is followed by another (for example at $t = 2500$).

3.2 Detailed description of the mechanisms of the intermittency

The suppression or growth of the quiescent variable is mainly governed by the magnitude of the active variable. The larger the time-average of the active variable, the greater the suppression (or smaller the growth) of the quiescent variable (for this choice of parameters). This is because of (for instance) the $-|z_2|^2 z_1$ term in the z_1 equation in (4). This suppression and growth, and the sets D^{in} etc., can be seen explicitly in figures 5 and 6. Figure 5 shows a detail from the time series in figure 3. The five marked segments are displayed in figure 6 as plots of $\text{Re}(z_1)$ (in black) and $\text{Re}(z_2)$ (in grey) against $\text{Im}(z_1)$ and $\text{Im}(z_2)$, and $|z_1|$ and $|z_2|$ against v. First in segment I we see the system heading into the nonlinear switching region. Here z_1 spirals in and z_2 spirals out to meet in a region in which the two variables are of similar magnitude. Since the parameters are symmetric it is a delicate issue which variable is favoured in the switching mechanism. Segment II shows the system favouring the dipole z_1 variable, and the system leads into the region D^{in}. Note that the similar magnitude of z_1 and z_2 causes the damping of the variable v via the $-(|z_1|^2 + |z_2|^2)$ term in the $\dot{v}$ equation. In segment III we have reached D^{in}, which is a periodic torus around the v-axis. This torus has a sufficiently large average $\langle |z_1| \rangle$ to suppress z_2 further. D^{in} unstable within $\mathcal{D}$ and in segment IV we see both the torus and v growing, leading to D^{out}. The set D^{out} can be seen in segment V, and is equivalent to the chaotic attractor shown in figure 2(b). This allows the growth of the quiescent variable because although $|z_1|$ reaches larger values, it also spends a long time much closer to the v-axis, and this results in a smaller average $\langle |z_1| \rangle$.

3.3 Breaking the $z_1 \leftrightarrow z_2$ symmetry

We can break the symmetry of the parameters in the linear growth term, for example, by setting $\sigma \neq 0$ to the equations. One might suppose, setting a greater rate of linear growth in z_1 leads to the z_1 (dipole) subspace being preferred, as when a switch is possible, when z_1 and z_2 are of comparable size, the direction with the greatest eigenvalue should dominate. However, it appears that the opposite can be true, at least for the parameter values we have investigated.
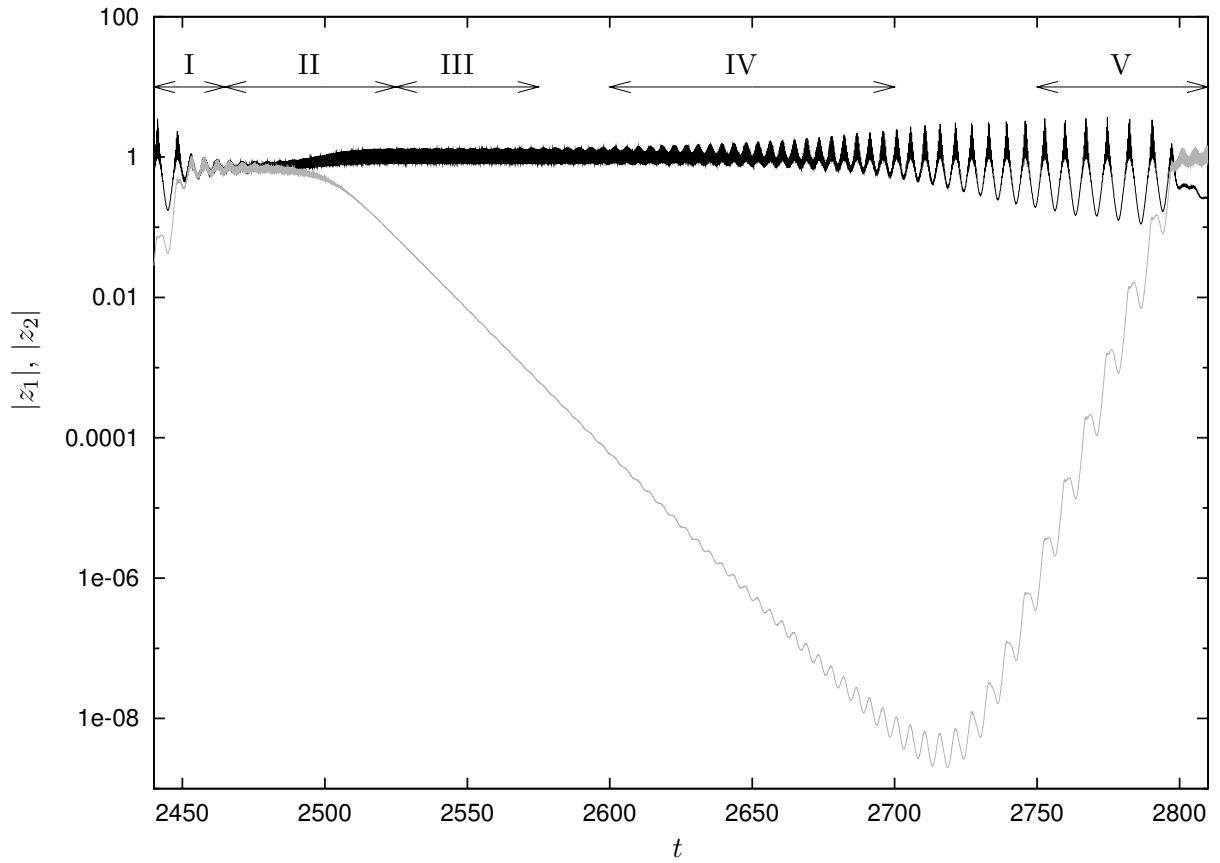
12

Figure 5: Close-up of the time series in figure 3 detailing the different episodes during a 'laminar phase' of the intermittency as the trajectory approaches the subspace $\mathcal{D}$.
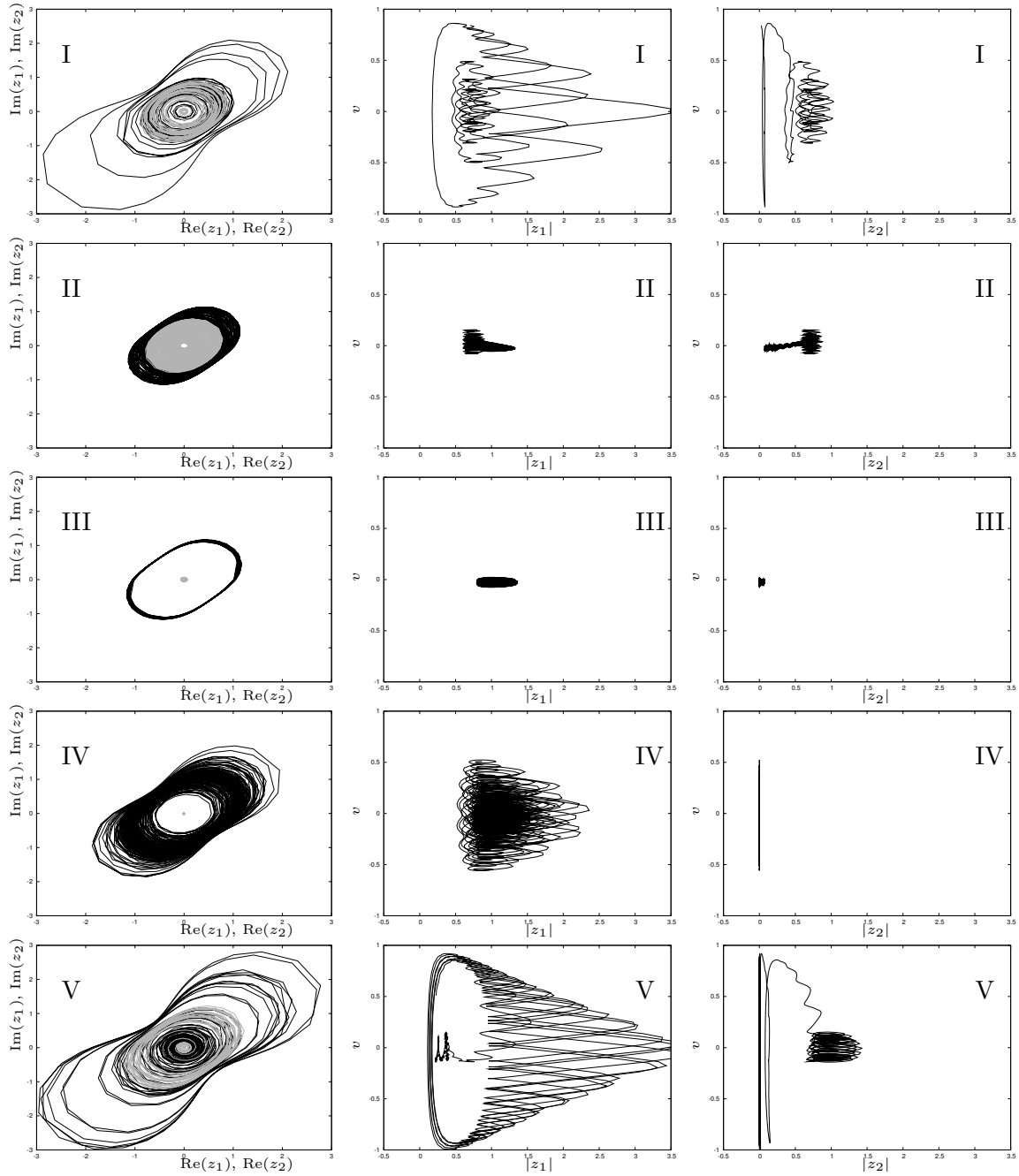
Figure 6: Projections of phase portraits of different time segments of figure 5 showing the different episodes of the in–out intermittency for the active variable z_1, while the quiescent variable z_2 decays and then grows. In the plots in the left column black lines represent z_1 and grey lines represent z_2. In I the trajectory is approaching the nonlinear switching region; II shows the trajectory leading into D^{in}; in III it is near D^{in}; IV shows it leading towards D^{out}; finally in V the trajectory is near D^{out}.
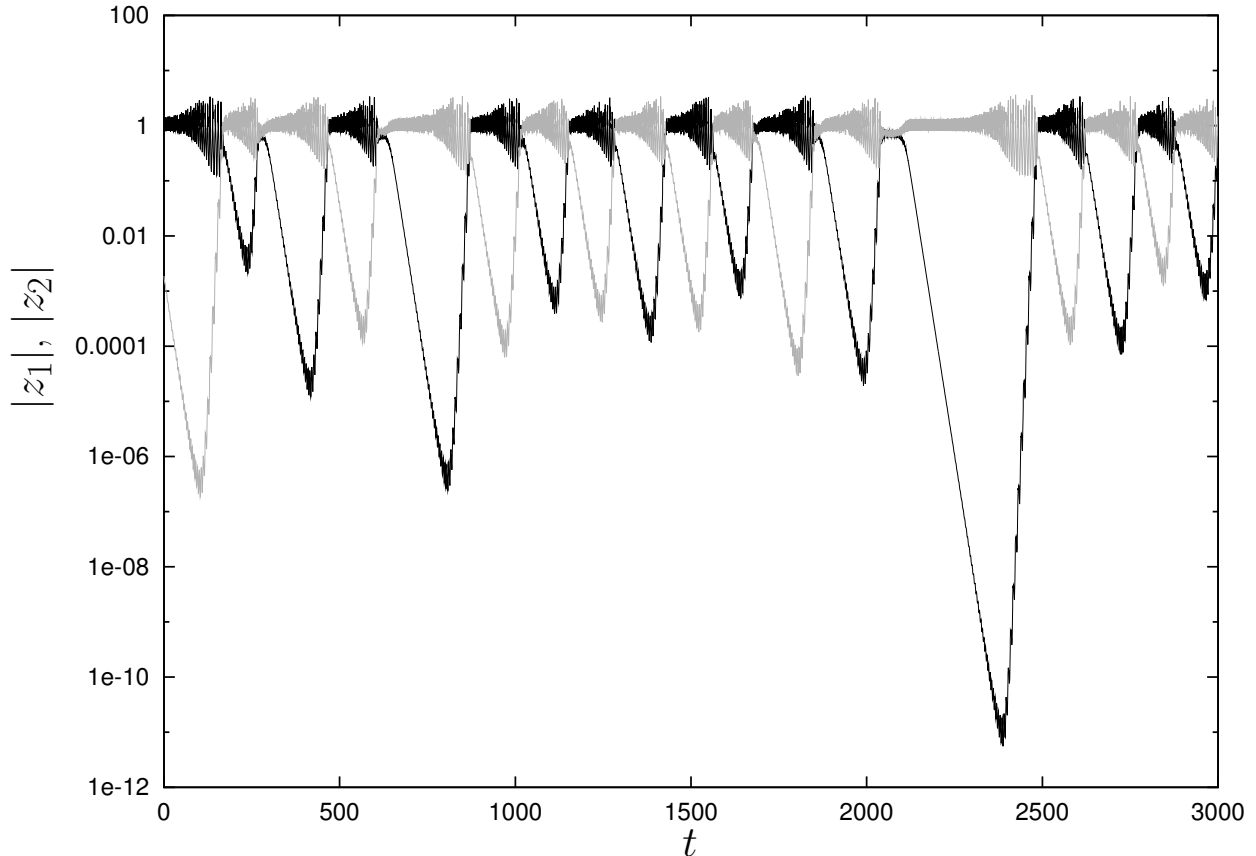
14

Figure 7: Time series as for figure 3, but with $\mu = 0.026$ and $\sigma = 0.001$. Here the linear growth rate is greater in the dipole variable. However, the quadrupole subspace is on average favoured.

Figure 7 shows a time series as in figure 3, but now with $\mu = 0.026$ and $\sigma = 0.001$, so the growth rate for z_1 is greater than that for z_2. The dynamics for these parameters starting with initial conditions solely in $\mathcal{Q}$ are equivalent to those given in figure 2(b) (or figure 2(a) for a more specific, and very precise, choice of initial conditions), and for initial conditions solely in $\mathcal{D}$ we have the dynamics in figure 2(c). For initial conditions not in either invariant subspace, a typical trajectory switches between these behaviours.

Despite the larger linear growth rate in z_1, the trajectory favours the activity in z_2. There are many factors involved in taking precedence over the linear growth rate. These include the transverse Lyapunov exponents at D^{in}, D^{out}, Q^{in} and Q^{out}; the tangential Lyapunov exponents at D^{in}, D^{out}, Q^{in} and Q^{out}; the average suppression from the active variable on the quiescent variable; the length of the laminar phases between switches; nonlinear effects within the switching mechanism; the type of attracting dynamics within the invariant subspaces (periodic or chaotic); other invariant or nearly-stable sets within the invariant subspaces. These are all important, but we will concentrate in section 4 on two — the length of laminar phases and the switching mechanism. We give results

15

to suggest that large bias towards dipole (resp. quadrupole) stems from an increased tendency in the switching mechanism to follow a dipole (resp. quadrupole) active phase with another.

3.4 Blowout bifurcation to intermittency

Consider a family of dynamical systems smoothly parametrized by some $\lambda \in \mathbb{R}$ with a proper invariant subspace N for all values of λ. If the dynamics in N is independent of λ we say λ is a normal parameter relative to N. As discussed in [2, 5] for normal parameters one can expect to locate blowout bifurcations relatively easily; for more general parameters this is not the case. An examination of the equations (4) reveals that for the invariant subspace $\mathcal{Q}$ the following are normal parameters

$$\sigma, \; \omega_1, \; \epsilon_1, \; d_1, \; b_1, \; \beta_1, \; \gamma_1, \; \tau, \; e$$

while for $\mathcal{D}$ the following are normal parameters

$$\omega_2, \; \epsilon_2, \; d_2, \; b_2, \; \beta_2, \; \gamma_2, \; \tau, \; e$$

In particular, only τ and e are normal for both subspaces. On varying these from the values (6) we can stabilise an attractor in the invariant subspace via a blowout bifurcation whilst leaving the dynamics within the subspace unaffected. The blowout appears to be subcritical and we find no cases where there are attractors that are for example stuck on to only one invariant subspace. Figure 8 illustrates the changes in typical dynamics on increasing τ. For $\tau < 1.5$ we find stable two-state in–out intermittency for typical initial conditions, as in figure 8(a). Increasing τ beyond 1.5 creates an attractor close to $z_2 = 0$ but bounded away from it, as in figures 8(b), (c) and (d) (here the initial conditions are chosen close to $\mathcal{D}$ - similar time series close to $\mathcal{Q}$ can be easily found with different initial conditions.) In figure 8(b) we have $\tau = 3.0$ and the resulting attractor has regular oscillations near $\mathcal{D}$. In 8(c) we have $\tau = 7.0$ and an aperiodic attractor, and in 8(d) $\tau = 8.0$ gives another oscillatory attractor of very long period. Increasing τ further causes these bounded attractors to give way to attracting dynamics within $\mathcal{D}$ (again for these initial conditions close to $\mathcal{D}$). Both figures 8(e) and 8(f) have $\tau = 10.0$ and the variable z_2 decays to zero. The different rates of decay is due to the different dynamics within $\mathcal{D}$ — in 8(e) the initial conditions lead to the chaotic attractor of figure 2(b), whereas in 8(f) the initial conditions lead to the periodic attractor of figure 2(a). As the parameters admit the permutation symmetry $z_1 \leftrightarrow z_2$ this means that the intermittency will be the same to both $\mathcal{D}$ and $\mathcal{Q}$ subspaces.

3.5 Influence of noise

Including additive noise in the model effectively destroys the invariance of the subspaces $\mathcal{D}$ and $\mathcal{Q}$. We introduce the noise by adding to each variable a random variable from a normal (Gaussian) distribution scaled with some noise level ξ, and with the square root of the previous time step. The results of this, for $\xi = 10^{-6}, \xi = 10^{-4}$ and $\xi = 10^{-3}$ are shown in figure 9. Small amounts of
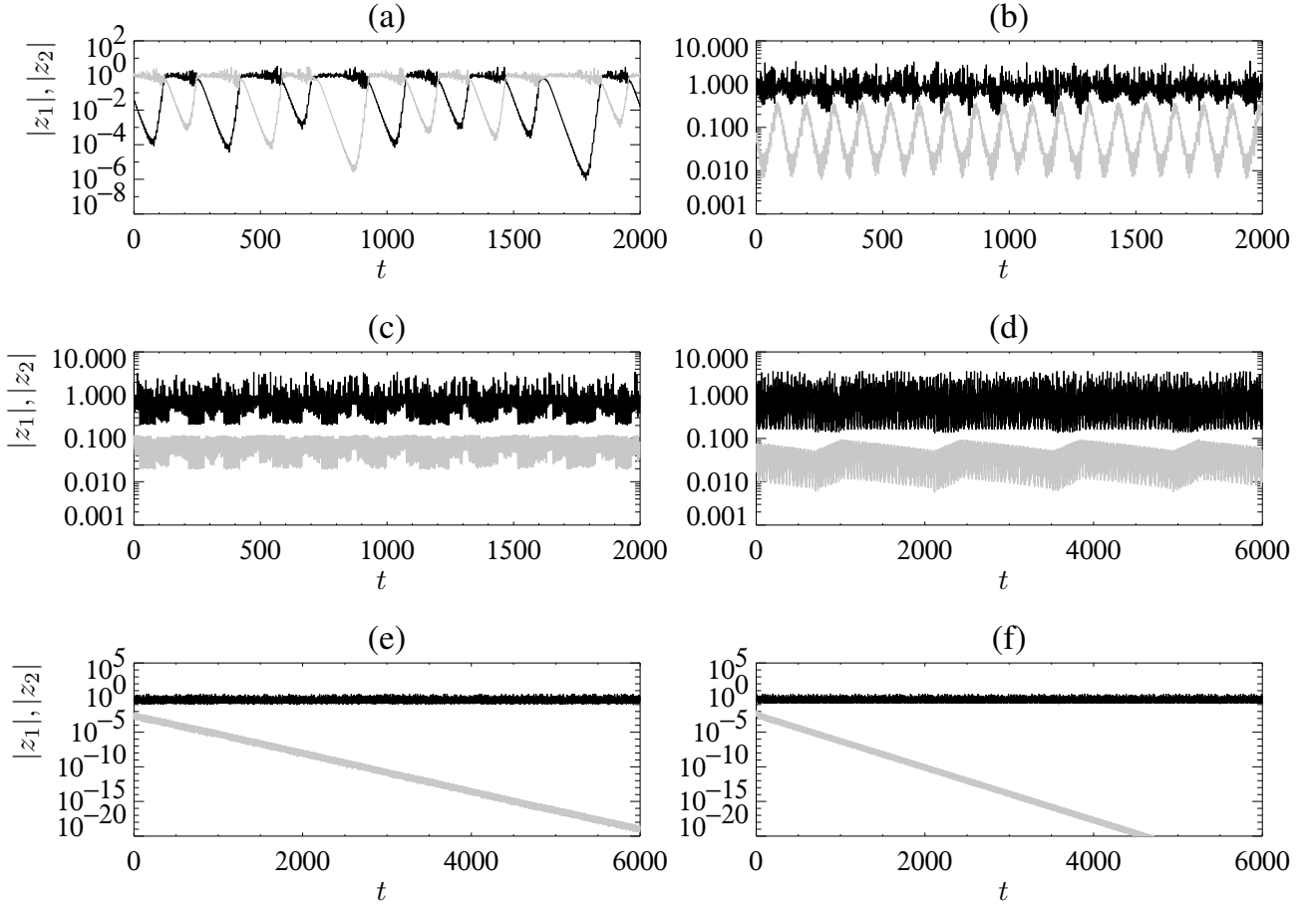
Figure 8: Dynamics for the symmetric parameters (6) and (7) on increasing τ. All figures plot $|z_1|$ in black and $|z_2|$ in grey. Figure (a) has $\tau = 1.0$, and shows stable two-state intermittent dynamics. Increasing τ beyond 1.5 creates an attractor close to $z_2 = 0$ but bounded away from it, as in figure (b), with $\tau = 3.0$. Increasing τ further causes this attractor to move closer to the invariant subspace $\mathcal{D}$, but remain bounded away from it. Figure (c) has $\tau = 7.0$. In figure (d) we have long period oscillatory behaviour, with $\tau = 8.0$. In figures (e) and (f) we have $\tau = 10.0$ and $\mathcal{D}$ has become attracting. Different initial conditions in (e) and (f) lead to different dynamics within $\mathcal{D}$. In (e) the initial conditions lead to the chaotic attractor of figure 2(b), whereas in (f) the initial conditions lead to the periodic attractor of figure 2(a). The larger average value of $|z_1|$ in this periodic orbit causes a much quicker decay in $|z_2|$.
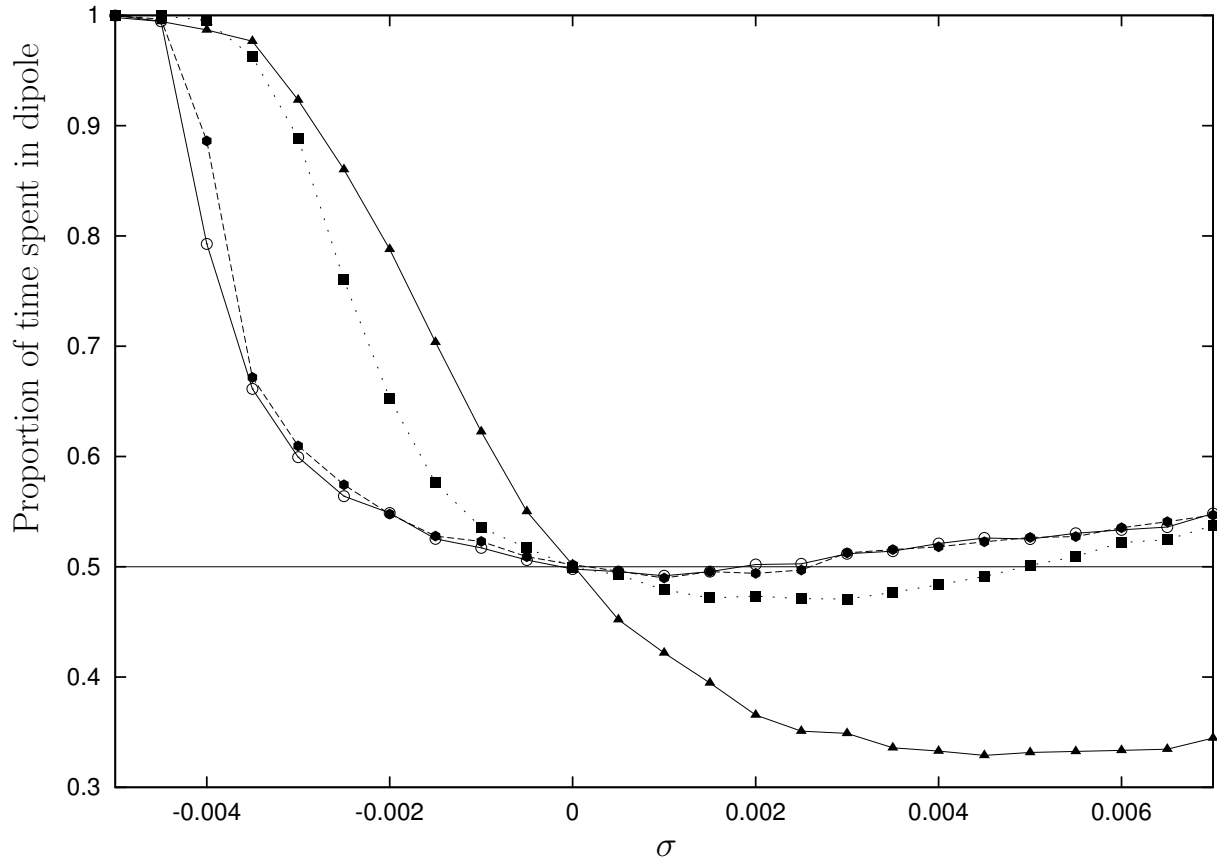
Figure 9: The effect of noise on the proportion of time spent near each invariant subspace. The data are produced by running a typical intermittent trajectory and recording the proportion of time that $|z_1| > |z_2|$, up to $t = 2 \times 10^6$ for each σ. The noise levels are $\xi = 0.0$ (empty circles), $\xi = 10^{-6}$ (solid hexagons), $\xi = 10^{-4}$ (squares), $\xi = 10^{-3}$ (triangles).

noise have, as expected, little effect on the proportion of time spent near each invariant subspace, but for larger ξ we find the effect on the proportion of time spent near a specific subspace upon breaking the symmetry of the parameters is even more pronounced. The behaviour of the laminar phases are not changed greatly by the addition of noise, but within the switching mechanism we see a greater tendency for the trajectory to be pushed towards $\mathcal{D}$ (say) many time in succession, without visiting $\mathcal{Q}$ (see section 4.1 and figure 12).

4   Modelling two-state intermittency as a Markov process

In the section we construct a probabilistic Markov chain model for the two-state intermittency observed in the the dynamics of the attractor (such as that in figure 3) where trajectories move between neighbourhoods of pure dipole and pure quadrupole invariant subspaces.
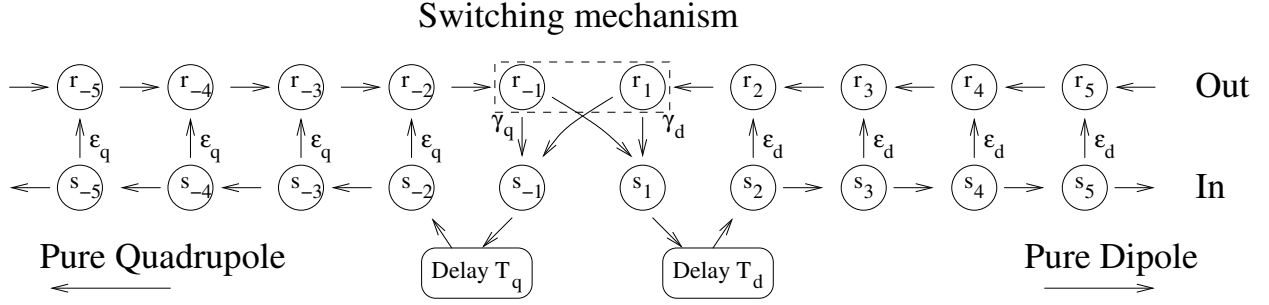
18

Switching mechanism

Figure 10: The Markov chain used to model the two-state in–out intermittency observed in the saddle-node/Hopf model. The states r_n and represent transverse distances $\rho^{|n|}$ from an invariant subspace near the 'out' dynamics while s_n represent transverse distances $\rho^{|n|}$ from the 'in' dynamics for some $0 < \rho < 1$. The switching mechanism is determined also by a random process with probabilities $\gamma_{d,q}$ and is subject to an additional delay of $T_{q,d} - 2$ steps, so the minimum time spent in the d,q chain is $T_{d,q}$.

Examining the dynamics of the intermittency, we note for example from figure 3 that the approach towards D^{in}, Q^{in} is approximately uniform, as is the departure from D^{out},Q^{out}. We therefore use a chain to model these as shown in figure 10 and assume that the leakage from the 'in' chain to the 'out' chain happens at a uniform rate $\epsilon_{d,q}$. We also assume that the switching mechanism is similarly governed by a Markov process parametrized by constants $\gamma_{d,q}$ and that there is a delay of $T_{d,q}$ steps during the switching mechanism.

The Markov model as shown in figure 10 has states that correspond to the intermittent model as follows: We model approach to D^{in} by a chain of states $\{s_n\}$, Q^{in} by a chain of states $\{s_{-n}\}$, D^{out} by a chain of states $\{r_n\}$, and Q^{out} by a chain of states $\{r_{-n}\}$, where we approach the relevant invariant set in the limit as $n \to \infty$. More precisely, there is a $\rho < 1$ such that for example p_n gives the probability of being approximately distance ρ^n from $\mathcal{D}$. If $P(a,b)$ is the probability of a transition from a to b we assume that within the chains, for $n \geq 1$

$$P(r_{n+1}, r_n) = 1, \quad P(r_{-n-1}, r_{-n}) = 1$$
$$P(s_{n+1}, r_{n+1}) = \epsilon_d, \quad P(s_{n+1}, s_{n+2}) = 1 - \epsilon_d$$
$$P(s_{-n-1}, r_{-n-1}) = \epsilon_q, \quad P(s_{-n-1}, s_{-n-2}) = 1 - \epsilon_q$$

for constants $\epsilon_{d,q} \in (0,1)$. All other transitions within the chains have zero probability, and all transitions take one time step, apart from the transition from s_1 to s_2 which takes $T_d - 2$ steps and from s_{-1} to s_{-2} which takes $T_q - 2$ steps. The transitions in the switching mechanism between the chains are assumed to have probabilities

$$P(r_1, s_1) = \gamma_d, \quad P(r_1, s_{-1}) = 1 - \gamma_d,$$
$$P(r_{-1}, s_{-1}) = \gamma_q, \quad P(r_{-1}, s_1) = 1 - \gamma_q,$$

for constants $\gamma_{d,q}$ also in $(0,1)$. The constants $\epsilon_{d,q}$ can be interpreted as the probability per unit time of leaking from the 'in' dynamics to the 'out' dynamics near the subspaces $\mathcal{D}, \mathcal{Q}$, and this gives rise to an exponential distribution of the durations that a trajectory is near the invariant subspaces after the constant delay $T_{d,q}$. The constants $\gamma_{d,q}$ correspond to the probability that the dynamics near the switching region send a trajectory that enters from $D^{\text{out}}, Q^{\text{out}}$ back into $D^{\text{in}}, Q^{\text{in}}$ respectively.

One can easily calculate the invariant probability p of the chain as

$$
\begin{aligned}
p(r_1) = p(s_1) &= A \\
p(r_n) = p(s_n) &= A(1-\epsilon_d)^{(n-2)}, \quad n \geq 2 \\
p(r_{-1}) = p(s_{-1}) &= B \\
p(r_{-n}) = p(s_{-n}) &= B(1-\epsilon_q)^{(-n+2)}, \quad n \geq 2
\end{aligned}
$$

implying that the residence time near each of the invariant subspaces is exponentially distributed. We have $p(r_n) = p(s_n)$ since the trajectories passing through r_n are precisely those that have previously passed through s_n. One can find that average residence times $A_{d,q}$ in the chains:

$$
A_d = T_d + 2\sum_{n=1}^{\infty} n\epsilon_d(1-\epsilon_d)^{(n-1)} = T_d + \frac{2}{\epsilon_d}
$$

and similarly $A_q = T_q + \frac{2}{\epsilon_q}$. Moreover, the transition between the q and d states at the end of the laminar phases is governed by γ_d and γ_q; observe that

$$
\begin{aligned}
A &= p(s_1) = (1-\gamma_q)p(r_{-1}) + \gamma_d p(r_1) = (1-\gamma_q)B + \gamma_d A, \\
1 &= A(T_d + 2/\epsilon_d) + B(T_q + 2/\epsilon_q)
\end{aligned}
$$

and so

$$
A = \frac{\epsilon_d \epsilon_q (\gamma_q - 1)}{2\epsilon_d(\gamma_d - 1) + 2\epsilon_q(\gamma_q - 1) + \epsilon_d \epsilon_q(\gamma_d T_q + \gamma_q T_d - T_d - T_q)}
$$

and there is a similar formula for B. The invariant probability density can be used to find the probability of a laminar phase in the 'dipole' and 'quadrupole' chains is

$$
P_d = \frac{1-\gamma_q}{2 - \gamma_d - \gamma_q}, \quad P_q = \frac{1-\gamma_d}{2 - \gamma_d - \gamma_q} \tag{8}
$$

giving the proportion of time spent in the 'dipole' and 'quadrupole' chains:

$$
M_d = \frac{P_d A_d}{P_d A_d + P_q A_q}, \quad M_q = \frac{P_q A_q}{P_d A_d + P_q A_q}. \tag{9}
$$

Note that, as discussed in Section 3.3, the relative proportion of visits to say the dipole subspace depend on both the average residence times $A_{d,q}$ and the probabilities of switching, namely $\gamma_{d,q}$.

One can verify the validity of the individual components of the Markov model for the original ODE problem. For example in figure 11 we show the distribution of the lengths of the laminar phases

σ	T_d	T_q	ϵ_d	ϵ_q	γ_d	γ_q
0	130	130	0.04254	0.04254	0.16215	0.16319
-0.003	159	176	0.04354	0.04214	0.45547	0.20377

Table 1: Numerical estimates for the Markov chain parameters. Observe that the greatest effect of the symmetry breaking term $\sigma = -0.003$ is to change the transition probabilities $\gamma_{d,q}$ within the switching mechanism.

for a long timeseries with (a) corresponding to figure 3 ($\mu = 0.026$, $\sigma = 0$) and (b) corresponding to $\mu = 0.026$, $\sigma = -0.003$. Note that the switching mechanism for the ODE takes a certain minimum time after which the frequency of occurrence drops off exponentially.

To estimate the proportion of time spent in near $\mathcal{D}$ and $\mathcal{Q}$ we take a threshold ($|z_1| < 10^{-2}$) to determine when we are close the invariant subspace and find the transition probabilities $\gamma_{q,d}$. These can be estimated by classifying the timeseries into $\mathcal{D}$ and $\mathcal{Q}$ phases and so associate the timeseries with a string $\{w_i\}_{i=1}^n$ with $w_i \in \{\mathcal{D}, \mathcal{Q}\}$. We can then estimate

$$\gamma_d = \frac{\#\{1 \leq i < n \ : \ w_i = w_{i+1} = \mathcal{D}\}}{\#\{1 \leq i \leq n \ : \ w_i = \mathcal{D}\}},$$

that is, γ_d is the frequency of observing $\mathcal{D}$ as the next laminar phase give that the previous one was $\mathcal{D}$. γ_q can be estimated similarly. Table 1 gives estimates of the parameters as computed from the timeseries (we take $T_{d,q}$ to the nearest integer for the discrete time Markov chain). Once having fitted the parameters $\epsilon_{d,q}$, $T_{d,q}$ and $\gamma_{d,q}$ one can use the model to predict for example using (9), the proportion of time spent near the dipole model. As an example, for $\sigma = 0$ we estimate M_d from the parameters and $\tilde{M}_d$ from a (different) timeseries and find

$$M_d = 0.4997, \quad \tilde{M}_d = 0.5023$$

for $\sigma = 0$, while

$$M_d = 0.5724, \quad \tilde{M}_d = 0.5760$$

for $\sigma = -0.003$.

4.1 Two-state in–out intermittency and noise

The details of the dynamics near the invariant subspaces for instance in Figure 3 reveals that the 'in' dynamics within $\mathcal{D}$ is periodic while the 'out' dynamics is chaotic, and so one could construct a model where the deterministic flow away from the invariant subspace is replaced by a biased random walk. This will not substantially increase the accuracy for this case, but in cases where the variance of the 'out' chain propagation is much larger it would be necessary; this would give a more sophisticated model than here or in [4]. Similarly, one could make the Markov model a lot
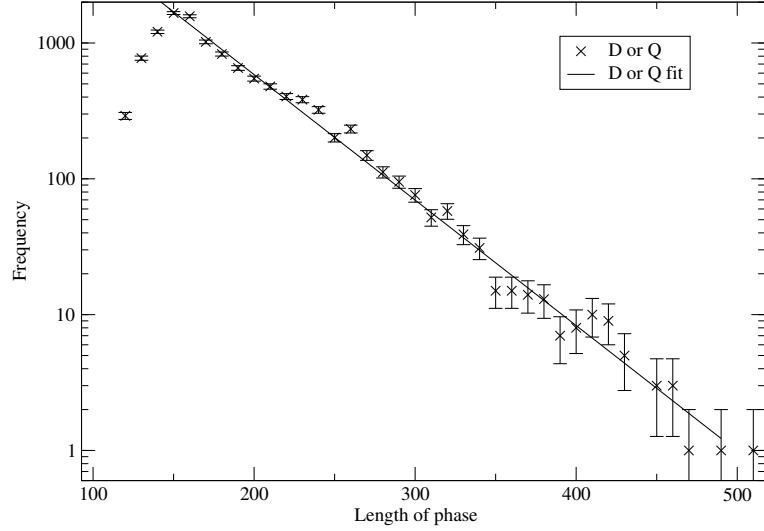
(a)
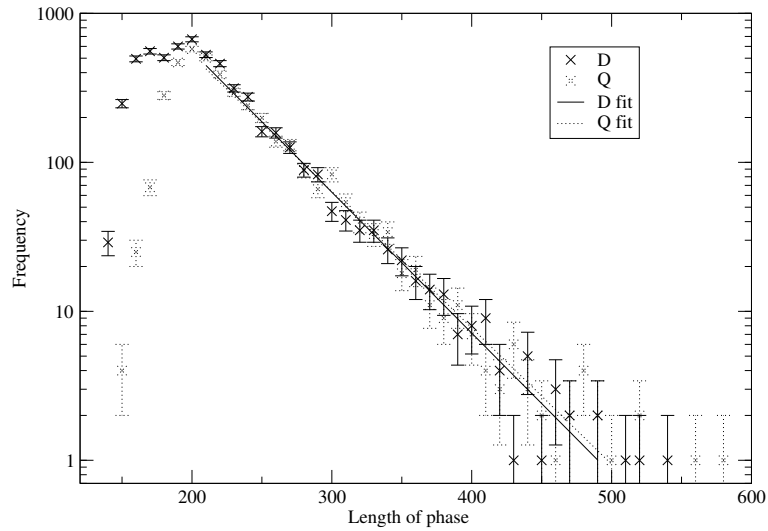
(b)

Figure 11: Distributions of the lengths of laminar phase T (near either $\mathcal{D}$ or $\mathcal{Q}$) subspaces for (a) the symmetric case shown in Figure 3 ($\mu = 0.026$, $\sigma = 0$) and (b) an asymmetric case $\mu = 0.026$, $\sigma = -0.003$. Observe that there is a good fit to a constant delay and an exponential probability distribution of phase length T in both cases where for (a) we have $P \sim e^{-0.02127T}$ for approaches to either, and (b) we have $P \sim e^{-0.02177T}$ for approaches to D and $P \sim e^{-0.02107T}$ for approaches to Q. Note that the lengths of laminar phases change very little.
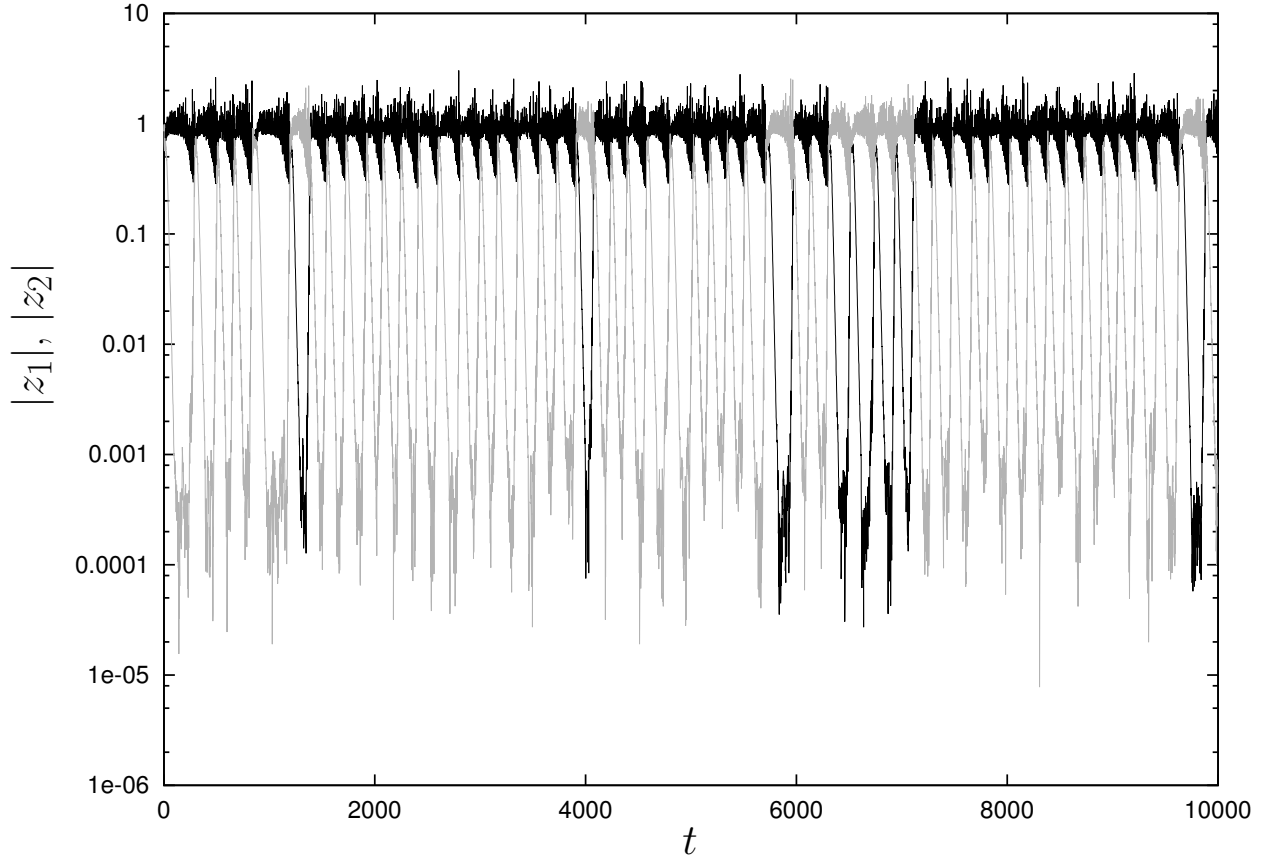
Figure 12: Time series showing intermittency in the presence of noise. The parameter values are as in figure 3, but with $\sigma = -0.003$ and $\xi = 10^{-4}$. The dipole subspace is greatly preferred because the transition probabilities in the switching mechanism now favour a dipole $\rightarrow$ dipole switch.

more sophisticated by including a continuum of states and by including noise effects along the lines of [4, 8, 25].

In fact, the introduction of noise to the system accentuates the findings of the above — that the greatest effect of the symmetry breaking term σ is to change the transition probabilities $\gamma_{d,q}$ within the switching mechanism. Figure 12 shows a time series showing the intermittency for $\sigma = -0.003$ and $\xi = 10^{-4}$, with the other parameters as before. Here it is clear that the dipole subspace is much favoured, and this bias is far more pronounced than with $\xi = 0$ (recall that for $\sigma = -0.003$, $\xi = 0$ we had $\tilde{M}_d = 0.5760$ — here $\tilde{M}_d = 0.8976$). It is clear that the tendency within the switching mechanism is now to follow a dipole active phase with another dipole phase, and in fact we can estimate the transition probabilities as before as $\gamma_d = 0.93467$ and $\gamma_q = 0.35801$.

5 Discussion and conclusions

In summary, we have examined a system that displays intermittent switching between chaotic dynamics in two invariant subspaces. In detail, the intermittency mechanism involves four states, two in each of the invariant subspaces. Two of these states ($\mathcal{D}^{\text{in}}$ and $\mathcal{Q}^{\text{in}}$) are transversely stable but unstable within the invariant subspaces. The other two ($\mathcal{D}^{\text{out}}$ and $\mathcal{Q}^{\text{out}}$) are transversely unstable but attractors within the invariant subspaces. Once the system moves away from the invariant subspaces, there is nonlinear switching and reinjection towards $\mathcal{D}^{\text{in}}$ and $\mathcal{Q}^{\text{in}}$. We have developed a Markov model of this intermittency mechanism that is capable of capturing the exponential distribution of times spent near each invariant subspace. This switching mechanism is a new feature of two-state intermittency that is not present in previous examples of in–out intermittency. Our work also sheds light on the switching behaviour observed in other dynamo models, for example the mean-field dynamo model [16] and the model of geodynamo reversals in [21]. In the latter case the switching mechanism seems to be be comparable to the mechanism in the present paper.

Although we have derived the model from perturbations near the codimension-two interaction of a saddle-node bifurcation with two symmetry-related Hopf bifurcations, and we have not included all possible interaction terms even up to cubic order, we presume (but cannot prove) that the dynamics we have described is robust or at least prevalent. We have used the degeneracy as an organizing centre to give dynamics that has two-state intermittency. The model we have considered is also physically motivated by consideration of hydrodynamic and magnetic instabilities — see for example [16]. In addition, the Hopf bifurcations to dipolar and quadrupolar dynamo activity often occur for similar (or even the same) parameter values in mean-field dynamo models, so it is reasonable to regard a notional symmetry between these Hopf bifurcations as being only weakly broken.

One of the most surprising results of this investigation has been the recognition that linear growth rates (or average residence times) near the invariant subspaces $\mathcal{D}$ and $\mathcal{Q}$ do not determine the average proportion of time spent close to the two subspaces. There are are many other factors that determine which of the two subspaces is preferred. The most important, at least for the Markov model, is the "switching mechanism" operating in the fully nonlinear regime that determines a preference of one phase to the other, once the equivalence of the two invariant subspaces is broken. We observe that switching can be greatly affected by the addition of noise.

As discussed in [6] and [7], numerical simulations of cycling chaos need to be carried out with great care. The simulations presented in this paper were performed to double precision accuracy using the Bulirsch–Stoer adaptive step integrator [27] with a relative tolerance of 10^{-8} at each time step. Rounding errors may force the dynamics into invariant subspaces, and care was taken to interpret correctly when this occurred. The dynamics of (4) was also simulated with the inclusion of small amounts of additive isotropic noise, in which case the effects of rounding into an invariant subspace could be easily avoided.

Acknowledgements

References

[1] V.S. Anishchenko, V.V. Astakhov, A.B. Neiman, T.E. Vadivasova and L. Schimansky-Geier. *Nonlinear Dynamics of Chaotic and Stochastic Systems* Springer series in synergetics, Springer Verlag Berlin (2002).

[2] P. Ashwin, J. Buescu, and I. Stewart. From attractor to chaotic saddle: a tale of transverse instability. *Nonlinearity* **9**, 703 (1996).

[3] P. Ashwin and P.J. Aston, Blowout bifurcations of codimension two. Physics Letters A **244**, 261-270 (1998).

[4] P. Ashwin, E. Covas and R. Tavakol. Influence of noise on scalings for in–out intermittency. *Physical Review E* **64**, 066204 (2001).

[5] P. Ashwin, E. Covas and R. Tavakol, Transverse instability for non-normal parameters. Nonlinearity **12**, 563–577 (1999).

[6] P. Ashwin, M. Field, A.M. Rucklidge and R. Sturman Phase resetting effects for robust cycles between chaotic sets. Chaos **13** 973–981 (2003).

[7] P. Ashwin and A.M. Rucklidge. Cycling chaos: its creation, persistence and loss of stability in a model of nonlinear magnetoconvection. Physica D **122** 134–154 (1998)

[8] A. Çenys, A.N. Anagnostopoulos, and G.L. Bleris. Distribution of laminar lengths for noisy on–off intermittency. *Phys. Lett. A* **224**, 346 (1997).

[9] E. Covas, R. Tavakol, P. Ashwin, A. Tworkowski and J.M. Brooke. In-out intermittency in PDE and ODE models of axisymmetric mean field dynamos. *Chaos* **11**, 404-409 (2001).

[10] M. Ding, and W. Yang. Stability of synchronous chaos and on–off intermittency in coupled map lattices. *Phys. Rev. E* **56**, 4009 (1997).

[11] H. Fujisaka, and H. Yamada. A new intermittency in coupled dynamical systems. *Prog. Theor. Phys.* **74**, 918–921 (1985); see also *Prog. Theor. Phys.* **75**, 1087 (1986).

[12] J. Guckenheimer and P. Holmes. *Nonlinear Oscillations, Dynamical Systems and Bifurcations of Vector Fields*, volume 42 of *Applied Mathematical Sciences*. Springer (1983).

[13] A. Hasegawa, M. Komuro, and T. Endo, *A new type of intermittency from a ring of four coupled phase-locked loops.* Proceedings of ECCTD'97, Budapest, Sept. 1997 (sponsored by the European Circuit Society).

[14] Yu. Ilyashenko and W. Li, *Nonlocal bifurcations* Mathematical surveys and monographs Vol 66, AMS, Providence RI (1999).

[15] V. Kirk. *Breaking of symmetry in the saddle-node Hopf-bifurcation. Phys. Lett A*, **154**,243 (1991).

[16] E. Knobloch, S. M. Tobias, and N.O. Weiss. Modulation and symmetry changes in stellar dynamos. *Mon. Not. R. Astron. Soc.*, **297**, 1123–1138 (1998).

[17] B. Krauskopf and B.E. Oldeman. *The saddle-node Hopf bifurcation with global reinjection* Preprint, University of Bristol (2003).

[18] B. Krauskopf and S. Wieczorek. Accumulating regions of winding periodic orbits in optically driven lasers. *Physica D* **173**:97–113 (2002).

[19] C. Martel, E. Knobloch and J.M. Vega, Dynamics of counterpropagating waves in parametrically forced systems. *Physica D* **137**, 94 (2000).

[20] Y.-C. Lai. Distinct small-distance scaling behavior of on–off intermittency in chaotic dynamical systems. *Phys. Rev. E* **54**, 321 (1996).

[21] I. Melbourne, M.R.E. Proctor and A.M. Rucklidge. A heteroclinic model of geodynamo reversals and excursions. In *Dynamo and Dynamics, a Mathematical Challenge* (eds. P. Chossat, D. Armbruster and I. Oprea) Kluwer: Dordrecht 363-370 (2001).

[22] E. Ott, and J. Sommerer. Blowout bifurcations: the occurrence of riddled basins and on–off intermittency. *Phys. Lett. A* **188**, 39 (1994).

[23] A. S. Pikovsky. On the interaction of strange attractors. *Z. Phys. B* **55**, 149 (1984).

[24] A. Pikovsky and M. Rosenblum and J. Kurths. *Synchronization: A universal concept in nonlinear sciences.* volume 12 of *Cambridge Nonlinear Science Series.* Cambridge University Press (2001).

[25] N. Platt, S. M. Hammel, and J. F. Heagy. Effects of additive noise on on–off intermittency. *Phys. Rev. Lett.* **72**, 3498 (1994).

[26] N. Platt, E. A. Spiegel, and C. Tresser. On-off intermittency: a mechanism for bursting. *Phys. Rev. Lett.* **70**, 279 (1993).

[27] W. Press, S. Teukolsky, W. Vetterling and B. Flannery. *Numerical Recipes in C.* Cambridge University Press (1988).

[28] S. M. Tobias, N. O. Weiss, and V. Kirk. Chaotically modulated stellar dynamos. *Mon. Not. R. Astron. Soc.*, **273**, 1150–1166 (1995).

[29] M. Woltering and M. Marcus. Riddled basins of coupled elastic arches. *Phys. Lett. A* **260**, 453–461 (1999).